Effects of different phase-matching conditions in sum-frequency-mixing systems in vapors

Sara Shepherd, Richard R. Moseley, Bruce D. Sinclair, and Malcolm H. Dunn
J. F. Allen Physics Research Laboratories, Department of Physics and Astronomy, University of St. Andrews, St. Andrews, Fife KY16 9SS, Scotland
(Received 6 July 1993; revised manuscript received 15 November 1993)

We have examined the effect of various phase-matching conditions on sum-frequency generation in vapors. Using sodium vapor two resonant-enhancement routes for sum-frequency mixing (SFM) via a second-order magnetic-field-induced nonlinearity were explored. On one route the output is resonant with a quadrupole-allowed transition and the other a dipole-allowed resonance. We will show that the first route is preferential for SFM as phase matching on this route is easier to control and we present results detailing the important parameters and their effect in focused and unfocused cases. A second-order nonlinearity of 0.5–1 pm V^{-1} is observed under optimum conditions. In the second route, variations in phase matching as one tunes across the transition may lead to a significant distortion of the spectroscopic line shapes. We show how the combination of different refractive-index sources can account for the different features seen.

PACS number(s): 42.65.Ky, 42.50.Hz

I. INTRODUCTION

Vapors can be useful media for second-order nonlinear processes if the intrinsic symmetry is broken by external means [1]. Transverse electric or magnetic fields, high-power pulsed excitation and noncollinear beams have been so used ([2], see references therein). To greatly increase the nonlinear susceptibility, three transitions are generally used for resonant enhancement and, in a closed atomic system, one must be dipole forbidden. Under such circumstances, electric-quadrupole transitions provide for efficient conversion and have low associated dispersion. Even at low vapor densities the refractive-index contribution from the dipole-allowed atomic lines may provide a significant phase mismatch, Δk, and control of this is of importance in such experiments. We use two contrasting sum-frequency mixing (SFM) schemes, differing in the placing of the low-dispersion quadrupole transition, to investigate phase-matching effects. We will show that the scheme in which the quadrupole transition is on the emission route exhibits only one major refractive-index contribution to the phase matching and hence is of more practical use in studying three-wave mixing. The added dispersion on the alternative route is shown to lead to considerable asymmetries in the output line profiles as a result of the more complex phase-matching situation.

Magnetic-field-induced three-wave mixing has been studied by several authors with regards to second-harmonic generation [2–7], sum-frequency mixing [8–10], and difference-frequency mixing [11]. Poustie and Dunn [10] investigated simultaneous single- and two-photon resonant SFM in sodium vapor using the $3S$-$3P$-$4D$ transitions. They examined the nonlinear process with the intermediate level tuned on and off resonance and presented phase-matching results. Using the $3S$-$3P$-$3D$ level scheme for more efficient conversion we extend this previous study, and in particular consider phase-matching behavior for both the plane-wave and focused beam cases. Variations in the phase-matched behavior of the focused case were studied in detail, and it can be seen to alter considerably as the focusing conditions are changed. These variations have been theoretically modeled and account for many apparent irregularities when comparing experimental results to those expected in theory. We then report an investigation of the $3S$-$3P$-$4P$ scheme in which the refractive-index contribution from the output transition ($4P$-$3S$) must now be included as well as that of one of the input transitions ($3S$-$3P$). This added source of phase mismatch leads to a complete distortion of the output line shapes away from those seen when the vapor density (and hence phase mismatch) is low. The line shapes are now strongly dependent on the exact detuning of the $3S$-$3P$ transition, and one of the Zeeman-split transitions to the ground-state level may dominate over the other, due to preferential phase matching. Which route predominates is dependent on the $3S$-$3P$ detuning.

In order to introduce our nomenclature for the systems studied consider the three-level atom shown in Fig. 1. In both schemes the levels 1 and 2 are the $3S$ and $3P$ levels of atomic sodium and the transitions between them are the well known, dipole allowed, sodium D lines. In the first scheme for sum-frequency mixing the third level is the $3D$ level of sodium, and the transition to this state from the $3P$ level is also a dipole-allowed transition. For this scheme the emission is via a quadrupole-allowed (dipole-forbidden) transition from the $3D$ to the $3S$ level. Due to this ordering of transitions we will refer to this route hereafter as the DDQ route. In the second scheme the third level is the $4P$ level of sodium and the transition to this level from the $3P$ level is not dipole allowed but is instead via a weaker quadrupole transition, while the emission from the $4P$ to the $3S$ levels is now dipole allowed. This second route will be called the DQD route to differentiate it from the one mentioned previously.

 ©1994 The American Physical Society

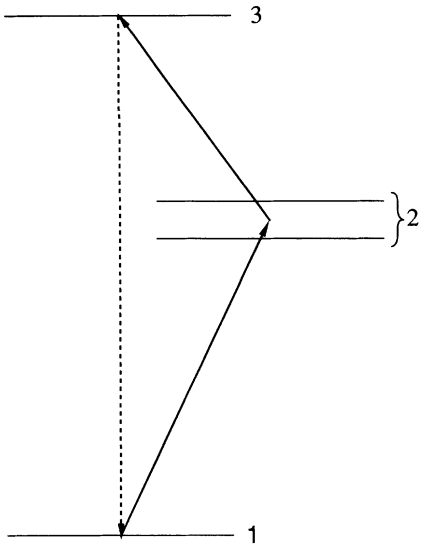

FIG. 1. A four-level atom with close middle levels, such as is produced by spin-orbit coupling in alkali metal vapors.

The refractive index associated with an atomic transition stimulated by a laser field of wavelength λ is calculated from the Sellmeier equation

$$n-1=\frac{\mathcal{N}r_e}{2\pi}\sum_j \frac{f_{ij}\alpha_i}{\frac{1}{\lambda_{ij}^2}-\frac{1}{\lambda^2}}, \tag{1}$$

where $\mathcal{N}$ is the atomic density, $r_e = 2.818\times10^{-15}$ m (the classical electron radius), and the sum over j covers all relevant upper levels. The subscript i denotes the lower level, hence f_{ij} is the oscillator strength of the transition, λ_{ij} the resonant wavelength of the transition, and α_i the fractional population of level i.

If one looks at the two mixing schemes for wavelength detunings away from single-photon resonance, then there is no significant transfer of population out of the ground, $3S$, state. For the DDQ route, the ground state is linked to the other two states by a strongly allowed dipole and a very weakly allowed quadrupole transition, only the first of which makes any contribution to the refractive index and hence phase mismatching. The contribution to the phase mismatch from this transition is shown in Fig. 2. Tuning the wavelength of this transition to values around and between the $3P$ lines allows regions of positive and negative Δk values to be probed, including a cancellation point between the lines where the phase mismatch is zero.

In contrast, for the dipole-quadrupole-dipole (DQD) route, the ground state is linked to each of the other two levels by a dipole transition, both of which contribute to the total phase mismatch, $\Delta k = k_3 - k_2 - k_1$, of the sum-frequency-mixing process. For our experiment, selection rules ($\Delta m_l = \pm1, \Delta m_s = 0$) allow two groups of Zeeman split transitions to occur in the $4P$-$3S$ transition, leading to a closely spaced doublet in the refractive-index curve, which is reflected in the contribution to Δk from this transition, Δk_3. This contribution to the overall phase mismatch by the $4P$-$3P$ dipole transition is

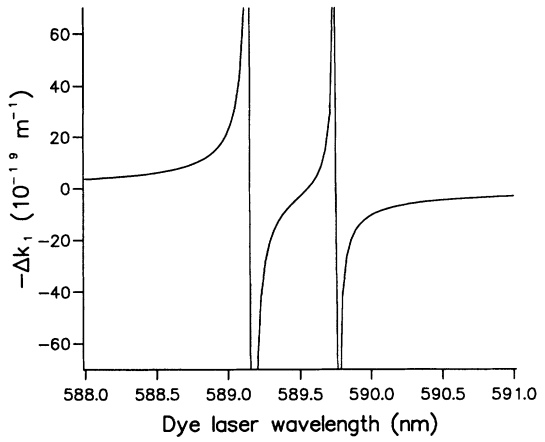

FIG. 2. Single-atom phase-matching contribution from the $3S$-$3P$ transition in sodium.

shown in Fig. 3. As either of the two contributing input wavelengths is scanned over two-photon resonance for this DQD scheme, the phase-matching contribution changes radically. This is superimposed on the static $3S$-$3P$ contribution in order to obtain the overall phase-matching conditions in the system. In this scheme it is no longer possible to have a constant phase mismatch during the scan, and novel effects in the line shapes, such as asymmetrical distortions and strong line dominance, are observed as a result in the output line shapes.

For simultaneous single- and two-photon resonance the DDQ route has an experimentally measured maximum effective nonlinearity of 0.5–1 pm V^{-1} (the uncertainty due to the parasitic absorption of the input waves), which is around twice that of KDP, and produced an ultraviolet emission on the quadrupole transition of 17 μW for our continuous-wave input powers of 140 and 300 mW. The powers produced in the DQD route were considerably lower due to lower matrix elements (about 1/25 that of the DDQ route). The advantages of using a vapor for frequency generation are that the vapor is self-repairing, and therefore scalable to high powers, and is transparent

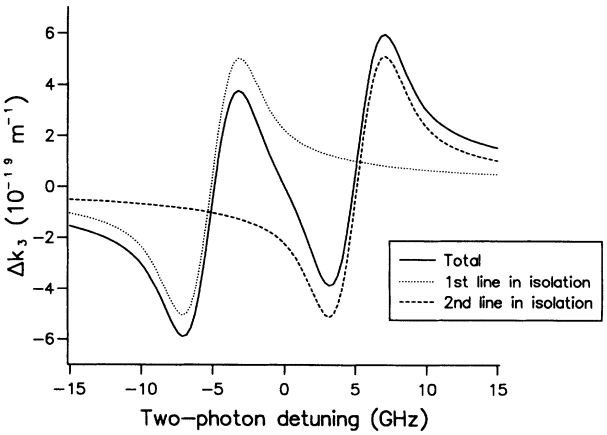

FIG. 3. Single-atom phase-matching contribution from the $3S$-$4P_{\frac{1}{2}}$ transition in sodium.

into the vacuum ultraviolet, unlike many nonlinear crystals. Control of the phase mismatch and an appreciation of its causes and effects are important for the design of a nonlinear optical frequency generator and the results detailed here relevant for any schemes with a similar system of allowed and forbidden transitions.

II. EXPERIMENT

We have used two single-frequency continuous-wave ring lasers to study the aforementioned routes in sodium vapor. A dye laser (Spectra-Physics 380D) provided light near 589 nm for the $3S$-$3P$ transition and a titanium sapphire laser (Schwartz Electro-Optic Titan, modified [12]) generated radiation near 819 nm (751 nm) for the $3P$-$3D$ ($3P$-$4P$) transition. The polarizations were aligned at 90° to the magnetic field, providing for $\Delta m_l = \pm 1$ (dipole) and $\Delta m_l = \pm 2$ (quadrupole) excitations. The beams were combined and passed collinearly through an oven containing sodium vapor and argon buffer gas (~ 1 mbar). The vapor region was nominally 10 cm long and the transverse magnetic field was generated by an electromagnet with 10-cm pole pieces. The input light was filtered off (2 UG11 filters, and an extra BG38 during DQD work) and coherent SFM emission detected by a photomultiplier tube (Hamamatsu 931B) with phase-sensitive detection used to raise the signal-to-noise ratio. Laser tuning and single-mode operation were monitored by 1.5-GHz confocal étalons, and absolute wavelength measured by a Kowalski style traveling wave meter and an iodine fluorescence cell.

III. SFM WITH ONE MAJOR PHASE-MISMATCH CONTRIBUTION (DDQ ROUTE)

For sum frequency generation via the $3S$-$3P$-$3D$ route the only significant source of dispersion is on the $3S$-$3P$ dipole transition. Hence, the overall phase mismatch, $\Delta k = k_3 - k_1 - k_2$, is given by the expression

$$\Delta k \approx -\Delta k_1 = \frac{-2\pi \Delta n(\omega_1)}{\lambda_1}, \tag{2}$$

where $\Delta n(\omega_1) = n(\omega_1) - 1$ is calculated from Eq. (1). For a plane wave the sum-frequency power produced by a vapor length, L, is given by

$$P(\omega_3) \propto \mathcal{N}^2 L^2 \frac{\sin^2\left(\frac{\Delta k L}{2}\right)}{\left(\frac{\Delta k L}{2}\right)^2}. \tag{3}$$

As the value of the phase mismatch is constant during a laser scan across two-photon resonance, the line shapes at a constant vapor density suffer no modulation due to phase matching. Typical experimental line shapes of the $3D$-$3S$ quadrupole transition as the magnetic field is increased are shown in Fig. 4. The expected theoretical behavior modeled using theory developed for SFM [12] from that used for second-harmonic generation [2,5] is shown in the same figure. The two can be seen to agree well.

As the vapor temperature is increased, the particle density increases also, a good description of the relation between the two being given by the empirical relation of Miles and Harris [13]:

$$\mathcal{N} = \frac{9.66084 \times 10^{24}}{T}\left(\exp\left[\frac{-12\,423.3}{T} + 17.3914\right]\right). \tag{4}$$

As the overall phase mismatch is proportional to vapor density, Eq. (3) can be rearranged by substituting $\Delta k = \mathcal{N}\Delta k'$, where $\Delta k'$ is the phase mismatch per unit atom, as given in Fig. 2,

$$P(\omega_3) \propto \frac{L^2 \sin^2\left(\frac{\mathcal{N}\Delta k' L}{2}\right)}{\left(\frac{\Delta k' L}{2}\right)^2}. \tag{5}$$

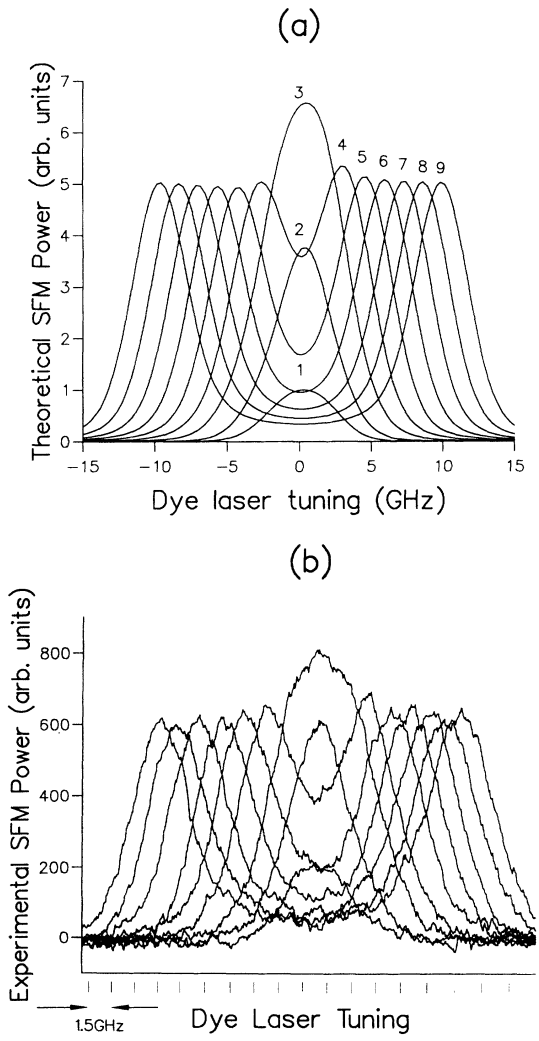

FIG. 4. Output line shapes: (a) theoretical and (b) experimental, for SFM on the $3S$-$3P$-$3D$ scheme for 0.0225, 0.045, 0.09, 0.135, 0.18, 0.225, 0.27, 0.315, 0.36 T magnetic fields, and are labeled 1 to 9 in this order on (a). Confocal marks of frequency separation 1.5 GHz are shown below the experimental spectra to provide a frequency scale.

This leads to the well known oscillatory behavior of output power with temperature [2,13], where the output power is proportional to the square of the sine of the number density. If the phase mismatch is zero then the oscillatory behavior vanishes and the output power is instead proportional to the square of the particle density. By selectively tuning the dye laser around the two $3P$ lines, the behavior of the sum-frequency power when the phase mismatch was either positive, negative or zero could be explored. The experimental and theoretical behavior were found to agree well. For the unfocused case the sign of the phase mismatch is irrelevant to the output power variation, and the laser tuning relative to the $3P$ lines determines the rate at which the phase mismatch increases. Figure 5 shows the change in output power with temperature for the point where Δk is zero, and a point where the mismatch is finite and positive. Unfocused laser beams were used to simulate plane-wave behavior and the Ti:sapphire laser was repeatedly tuned across resonance during the scans so as to always register the maximum power. The practical advantage of the phase-matching position is clearly seen and very high conversion efficiencies could be produced at high temperatures. The theoretical fit is a good functional one, the experimental vapor temperatures being adjusted smoothly to fit the curves due to the changing difference between measured temperature and actual temperature in the oven. The ability to precisely phase match is an important advantage of systems with a split central level.

When the input beams are focused into the vapor, the behavior of the phase-matched oscillations can be seen to alter. Using the theory developed by Lago, Hilber, and Wallenstein [14], we have simulated the predicted output power at the sum frequency with regard to certain key parameters. These parameters are the phase mismatch, the ratio of the length of the vapor to the confocal parameters of the two beams, ξ_1 and ξ_2, and the position of the focus within the vapor. The optimum conversion of power to the sum frequency was found when the two beams were focused into the vapor oven using a 20-cm focal length lens. As the waists of the dye and Ti:sapphire laser beams were 649 and 913 μm respectively, the focusing parameters were $\xi_1 = 2.7$ and $\xi_2 = 4$. This is in line with the expected optimum condition of $\xi = 2.8$, as predicted by Boyd and Kleinman [15]. Although the focusing parameters were unequal, we calculated, using the theory of [14], that this had little effect until the discrepancy was far larger than the case for our single lens experiment.

Figures 6 and 7 show typical traces of the behavior under optimum focusing for regions of positive and negative phase mismatch with the expected theoretical behavior for beams focused in the center of the oven. As expected, due to the phase shift of the Gaussian beams on passing through a focus, the power in the focused case reaches its first maximum at a lower vapor temperature than in the unfocused case for a positively dispersive region, and at a higher temperature for a negatively dispersive region. This is due to the accumulation of a π phase lead in the sum-frequency output wave from the two input waves and its own propagation through a focus. However, the form of the curves as the temperature was increased could not be straightforwardly predicted. In particular, the curves for negatively dispersive regions were often quite different from those expected, while the positively dispersive regions were found to be a more reasonable fit to theory. The factors which most affected the form of the phase-matching curves were found experimentally to be the focusing parameter ξ, the sign of the phase mismatch, the position of the focus, the uniformity of the vapor density in the oven, and the collinearity of the two beams.

Of these, the effects of the first two are shown in the previous figures and experimental and theoretical predictions agree qualitatively. A large part of the apparent deviation can be explained via the change in the position of the focus. Any asymmetry of the vapor density along the length of the oven can be expected to have a similar effect, with the power generated at the sum frequency not being symmetrically distributed around the focus, and hence exact cancellation will not occur at the points of phase-mismatch minima. Figure 8 shows the theoretically predicted power variations with temperature as the

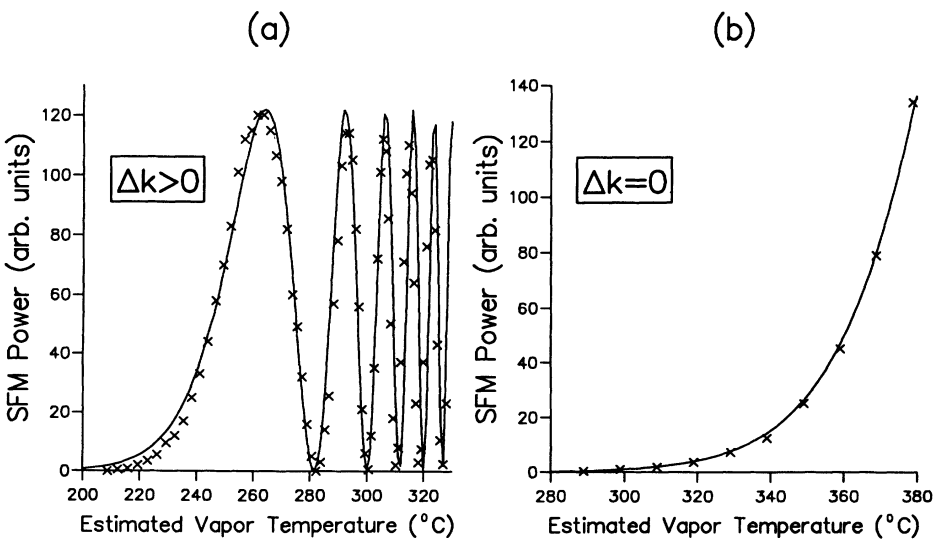

FIG. 5. Plane-wave phase-matching behavior with increasing particle density on the DDQ route for (a) $\lambda_1 = 588.57$ nm ($\Delta k > 0$) and (b) $\lambda_1 = 589.4$ nm ($\Delta k = 0$).

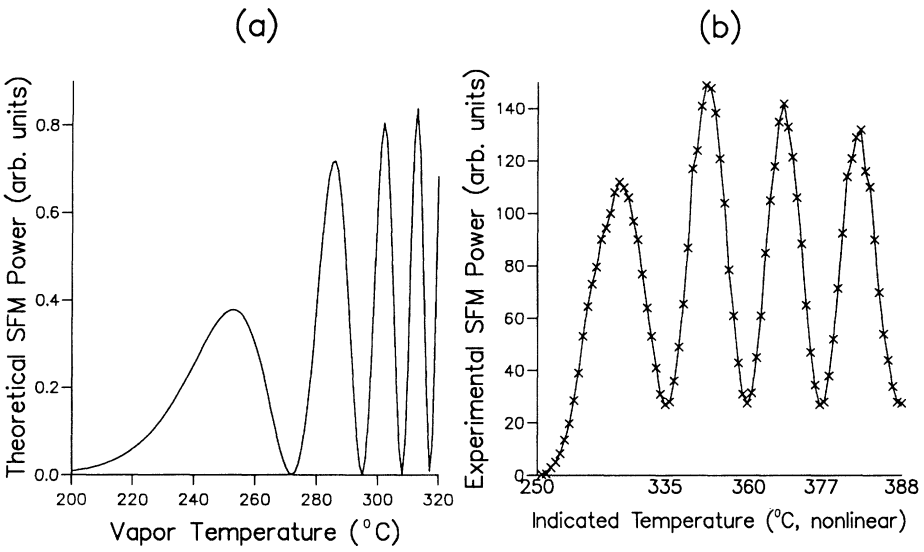

FIG. 6. Theoretical (a) and experimental (b) phase-matching behavior with focused input beams, using a 20-cm lens, for $\Delta k > 0$ (the line drawn through the experimental points is to aid the eye only).

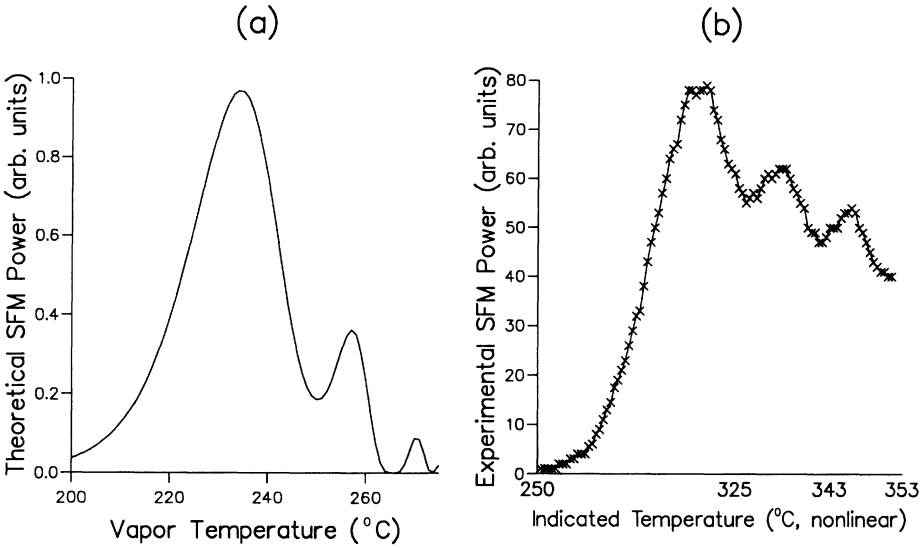

FIG. 7. Theoretical (a) and experimental (b) phase-matching behavior with focused input beams for $\Delta k < 0$ and using a 20-cm lens.

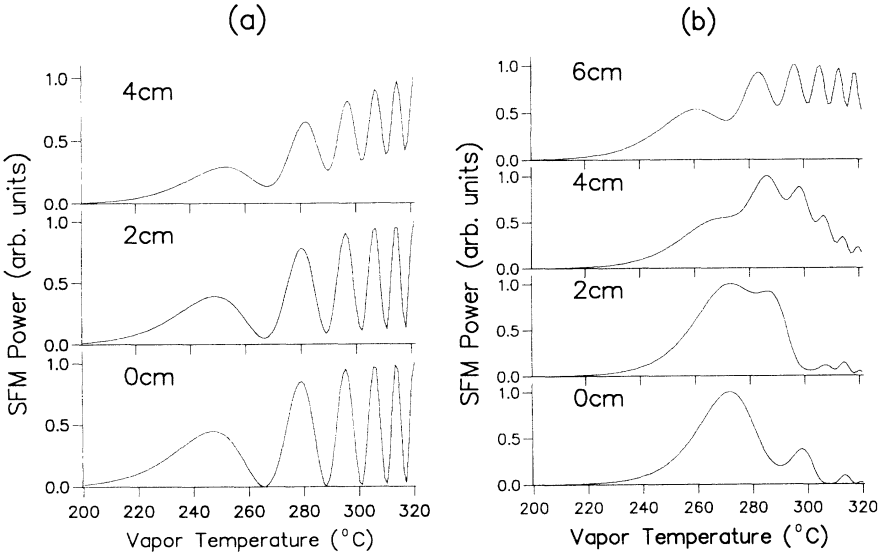

FIG. 8. Theoretical phase-matching behavior as the position of the focus is moved within the vapor relative to the center for (a) $\Delta k > 0$ and (b) $\Delta k < 0$.

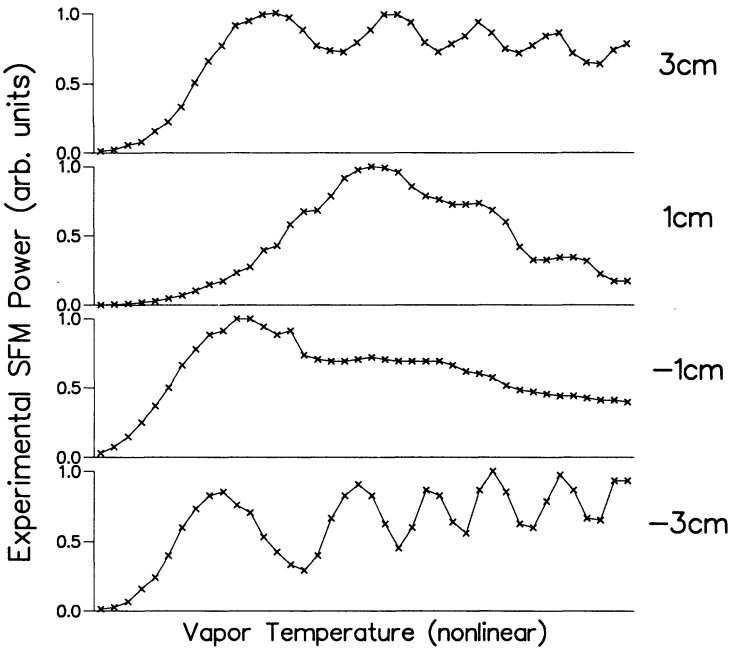

FIG. 9. Experimental phase-matching behavior as the focus is moved within the vapor relative to the center of the cell for $\Delta k < 0$, the central case being Fig. 7(b).

focus is moved away from the center of the oven for Δk positive and Δk negative regions. The experimentally observed behavior for a Δk negative position as the focus is moved to various positions away from the center of the oven is shown in Fig. 9, measured there, as the effect is more radical in this region. The experimental and theoretical curves show striking similarities, but the ideal, centrally focused, uniform vapor density, case was not observed, suggesting a residual vapor asymmetry in our apparatus.

The curves, however, still have some unexplained content tending to blur the features, leading to poor contrast zeros, especially in the negative phase-mismatch regime. This blurring factor was found to be a radial change in phase mismatch across the sum-frequency beam. The origin of this is uncertain, but vapor asymmetries and beam distortions are possible sources, as the theoretical models assume Gaussian input beams and no variation in vapor density radially across the generation region. The radial variation was clearly seen by using a charge-coupled-device (CCD) camera to determine the output beam profile, and relevant cross sections are shown in Fig. 10. At low vapor densities, before phase mismatching became important, a monotonic Gaussian-like cross section was seen. However, at above a few phase-mismatch oscillations a ringlike structure around a central maximum could be observed expanding outwards as the vapor density was further increased. This effect appears to be a product both of the focusing and the collinearity of the input beams, as the ring structure could be changed to a fringe structure by misalignment of the two input laser beams. If a small sample of the beam is taken by a pinhole, then the output power behavior looks more like that expected for a focused beam with good contrast minima supporting the case for a radial, as opposed to a longitudinal, blurring effect. Variations at different radial positions acted as though they were experiencing different phase mismatches and the integration over them—relevant to the total beam power—would account for the last discrepancies between theory and experiment as shown in the figures above.

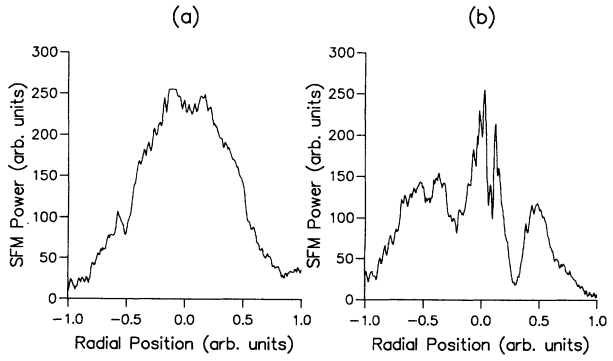

FIG. 10. Cross sections through the SFM output beam at (a) a low temperature (below the first phase-match peak) and (b) a higher temperature (well above the first phase-match peak).

IV. SFM WITH TWO MAJOR PHASE-MISMATCH CONTRIBUTIONS (DQD ROUTE)

The second SFM level scheme, $3S$-$3P$-$4P_{\frac{1}{2}}$, is shown in Fig. 11. Zeeman splitting leads to two strong resonant enhancement clusters, which for polarization perpendicular to the field were governed by the $\Delta m_l = \pm 1$ selection rule. Observed powers were lower on this route, largely due to lower matrix elements for two of the transitions, but the output was still readily observable. The $4P_{\frac{3}{2}}$ state is 168 GHz above the $4P_{\frac{1}{2}}$ state and so is sufficiently detuned to be neglected.

The refractive index, and hence Δk, now change across the two-photon resonance point as there is a dipole-

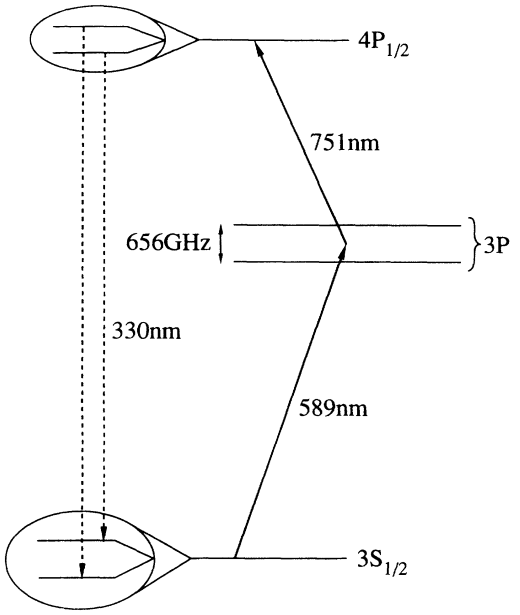

FIG. 11. The DQD scheme used, the $3S$-$3P$-$4P_{\frac{1}{2}}$ levels in sodium.

allowed transition to the ground state, leading to a phase-mismatch contribution, Δk_3, as shown in Fig. 3. It is important to note that when the two refractive-index resonances are added the resultant effect is an asymmetrical profile, as is highlighted by the isolated resonance curves shown in the same figure, and this leads to some of the observed effects. The tuning of the dye laser relative to the D lines then provides an adjustable offset, by changing Δk_1, on the total phase mismatch, $\Delta k = \Delta k_3 - \Delta k_1$. When the dye laser is tuned during the experiment Δk_1 may also vary slightly during the scan, tending to tilt the phase-matching curve slightly. Two possible phase-mismatch curves are shown in Fig. 12. In (a), case 1, the offset from the $3S$-$3P$ contribution is larger than the $3S$-$3D$ modulation and phase matching is never achieved. However, in (b), case 2, the tuning of the dye laser is such that one resonance only crosses perfect phase matching and this line will be preferentially generated.

At low particle densities it is possible to observe the line shape of the output relatively free from phase-matching effects. The predicted line profile was calculated, including the phasing and strength of the excitation and emission routes [12], in a similar model to that used for the DDQ route line shapes, and hence is wider than merely two Doppler broadened line shapes at the relevant Zeeman splitting and shows some asymmetry. Figure 13(a) shows these theoretical line shapes, while the experimental observation of them at low temperatures, for the laser tuning of case 1, is displayed in Fig. 13(b). It can be seen that the two show very good agreement, with only minor phase-matching distortions on the experimental curves.

In order to predict the output line shapes at higher temperatures, the line-shape model was altered to include the dispersion at each point during the scan, and the predicted line profile modulated for focused phase-matching behavior, using the approach of Boyd and Kleinman [15]. (Focusing was necessary to gain a readily detectable coherent SFM signal with the strong phase-matching effects.) At higher temperatures the profiles are strongly modulated by the phase-matching curve, and Fig. 14 compares theory to experiment when phase-mismatching effects are strong for the laser tuning of case 1, in which perfect phase matching is never achieved. There is good general agreement with distortions present and uneven peak heights. The fine detail of the phase-matching oscillations is lost in the experimental case due to the blurring effects of the radial function, as noted previously.

A very different regime is that of case 2 [i.e., the phase-mismatch behavior of Fig. 12(b)]. Theoretical predictions for this case, where one peak crosses perfect phase matching, are shown in Fig. 15. At lower temperatures, distortions and a slight height advantage are noted [Fig. 15(a)], while at higher temperatures the phase-matched peak dominates very strongly [Fig. 15(b)]. The experimental results which are presented in Fig. 16 show the strong peak dominance around the zero point, in good agreement with the theoretical predictions. Again fine detail is lost but the dominance of the phase-matched peak is clearly visible. If instead the other line is preferentially phase matched, by tuning the dye laser to the other side of the crossover in Δk_1 (Fig. 2), an equivalent

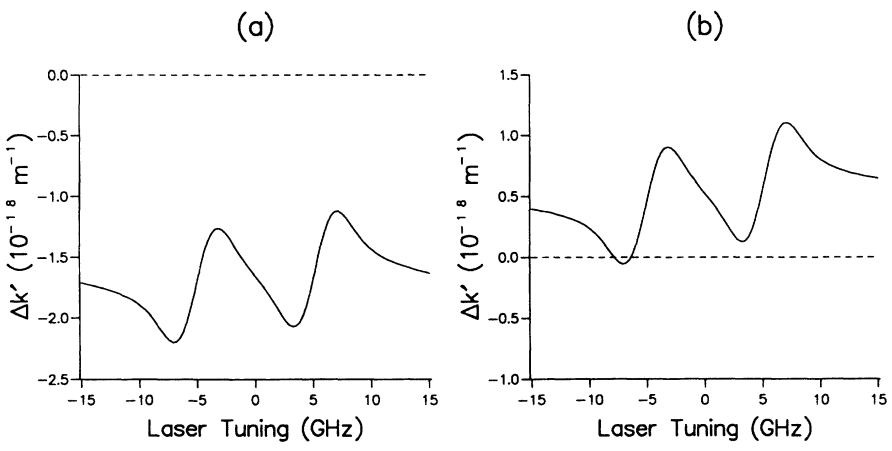

FIG. 12. Single-atom phase-mismatch curves for the DQD route at (a) $\lambda_1 = 588.96$ nm (case 1) and (b) $\lambda_1 = 589.440$ nm (case 2).

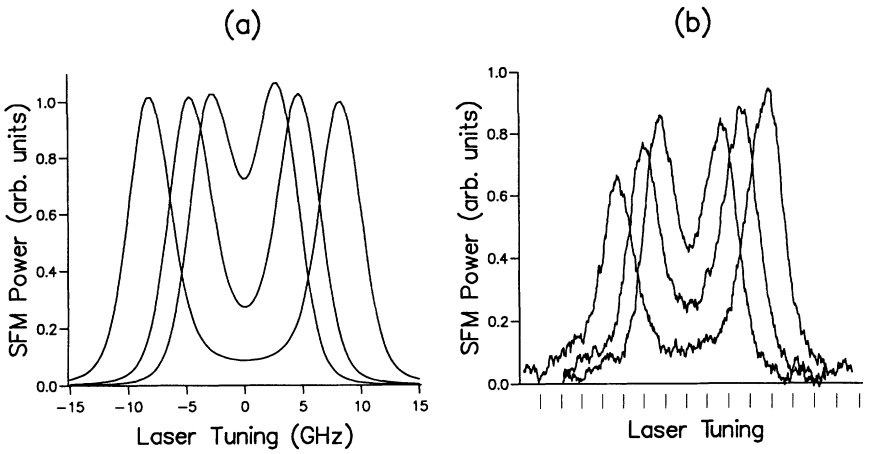

FIG. 13. Output line shapes: (a) theoretical and (b) experimental, for the $3S$-$3P$-$4P_{\frac{1}{2}}$ scheme at 0.18, 0.27, 0.45 T magnetic fields (splitting sequentially outwards) at temperatures below where phase matching becomes important. (Markers from a confocal of free spectral range of 1.5 GHz are shown below the experimental lines here, and in the following experimental figures as a frequency scale.)

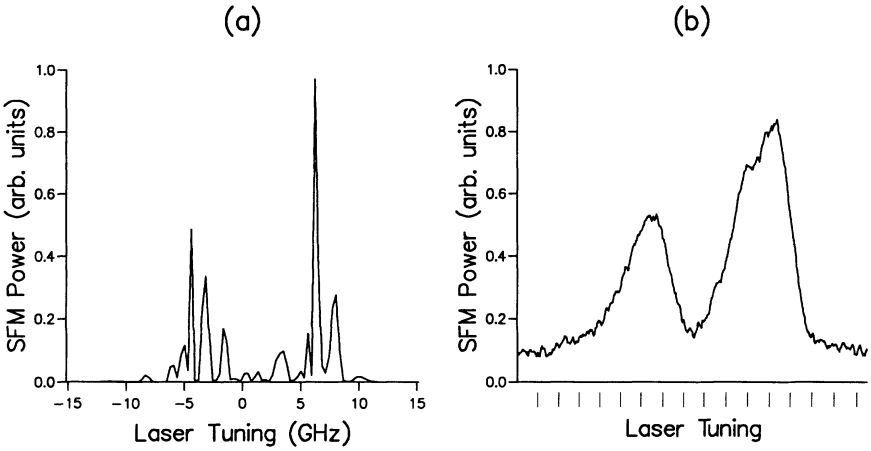

FIG. 14. Theoretical (a) and experimental (b) line shapes for case 1 at around 300 °C.

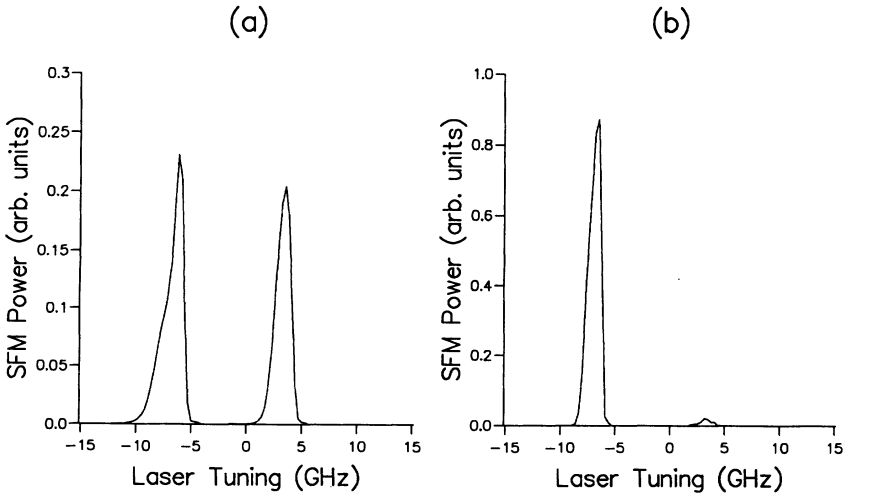

FIG. 15. Theoretical predictions of the modulated line shapes in the DQD route for the phase-matching curve of case 2 at (a) 260 °C and (b) 300 °C.

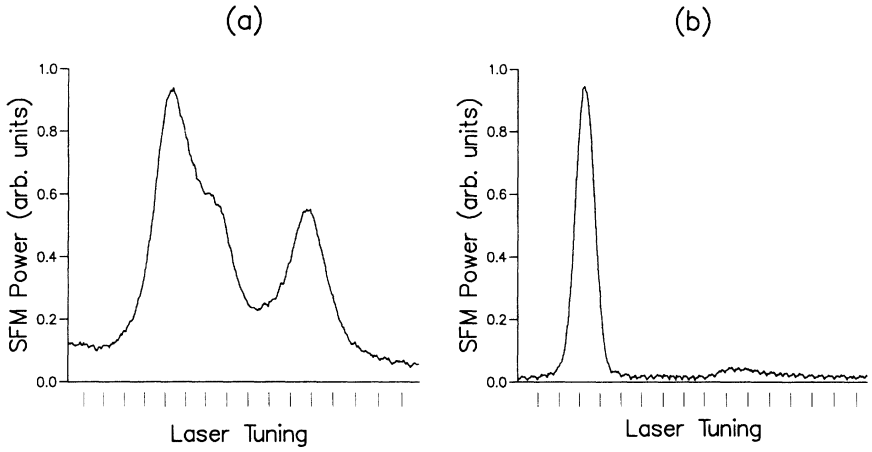

FIG. 16. Experimentally measured SFM line profiles at wavelengths and temperatures close to those used in Fig. 13.

line shape is expected, but with the other line in dominance. This was experimentally verified. The contrast in line strengths at these points is surprisingly strong and the spectra produced very different from the line shapes calculated without including the effects of phase mismatch, illustrating the importance of phase matching for the vapor densities typically used to get strong sum-frequency powers of $10^{20} \rightarrow 10^{21}$ m^{-3}.

V. CONCLUSION

We have compared two routes for second-order sum-frequency mixing, concentrating on the macroscopic phase-matching properties of the two routes. The two routes differ in the ordering of the three (two dipole, one quadrupole) transitions in the three-wave mixing. The ability to access areas of positive, negative, and zero dispersion in the DDQ route both for plane and focused waves has been demonstrated, and was used to investigate the various experimental variables which affect phase matching in vapors. Furthermore, we have shown in the DQD route how strong modulations of the output line shapes are produced by the changing phase mismatch as the emission is scanned through two-photon resonance, and how one Zeeman component can be preferentially phase matched and dominate strongly in the observed spectra. This makes the first (DDQ) route preferable, not just because the product of its matrix elements results in larger powers in the ultraviolet, but also because the phase matching on this route can be controlled and set to a constant positive, negative, or zero value. In studies where three-wave mixing is used to look at other atomic processes, the distortions on the DQD route type, due to phase matching, would tend to obscure less dominant effects. The maximum power obtained in the uv on the DDQ route was 17 μW, and by use of electromagnetically induced transparency it should be possible to extend the output by over two orders of magnitude [16]. While we have concentrated on SFM on the two particular routes probed experimentally, this work has applications in any second-order nonlinear wave-mixing process in a vapor.

ACKNOWLEDGMENTS

Two of us (R.M. and S.S.) wish to acknowledge personal support from The Carnegie Trust for the Universities of Scotland and SERC, respectively.

[1] N. Bloembergen, *Nonlinear Optics* (Benjamin, New York, 1965).
[2] B. D. Sinclair and M. H. Dunn, Phys. Rev. A **34**, 3989 (1986).
[3] T. Mossberg, A. Flusberg, and S. R. Hartmann, Opt. Commun. **25**, 121 (1978).
[4] M. Matsuoka, H. Nakatsuka, H. Uchiki, and M. Mitsunaga, Phys. Rev. Lett. **38**, 894 (1977).
[5] H. Uchiki, H. Nakatsuka, and M. Matsuoka, J. Phys. Soc. Jpn. **52**, 3010 (1983).
[6] M. H. Dunn, Opt. Commun. **45**, 346 (1983).
[7] B. D. Sinclair and M. H. Dunn, J. Mod. Opt. **35**, 517 (1988).
[8] A. Flusberg, T. Mossberg, and S. R. Hartmann, Phys. Rev. Lett. **38**, 694 (1977).
[9] D. S. Bethune, R. W. Smith, and Y. R. Shen, Phys. Rev. A **17**, 277 (1978).
[10] A. J. Poustie and M. H. Dunn, Phys. Rev. A **47**, 1365 (1993).
[11] A. Flusberg, T. Mossberg, and S. R. Hartmann, Phys. Rev. Lett. **38**, 59 (1977).
[12] S. Shepherd, Ph.D. thesis, University of St. Andrews, St. Andrews, Scotland, 1993 (unpublished).
[13] R. B. Miles and S. E. Harris, IEEE J. Quantum Electron. **QE-9**, 470 (1973).
[14] A. Lago, G. Hilber, and R. Wallenstein, Phys. Rev. A **36**, 3827 (1987).
[15] G. D. Boyd and D. A. Kleinman, J. Appl. Phys. **39**, 3597 (1968).
[16] R. R. Moseley, B. D. Sinclair, and M. H. Dunn, Opt. Commun. **101**, 139 (1993).